Construction of Symbolic Dynamics from Experimental Time Series

K. Mischaikow
School of Mathematics
Georgia Institute of Technology
Atlanta, GA 30332 USA
mischaik@math.gatech.edu

M. Mrozek
Instytut Informatyki
Uniwersytet Jagielloński
30-072 Kraków, Poland
mrozek@ii.uj.edu.pl

J. Reiss
School of Physics
Georgia Institute of Technology
Atlanta, GA 30332 USA

A. Szymczak
School of Mathematics
Georgia Institute of Technology
Atlanta, GA 30332 USA
andrzej@math.gatech.edu

May 7, 1998

Abstract

Symbolic dynamics plays a central role in the description of the evolution of nonlinear systems. However, there are few reliable methods for determining the symbolic dynamics of chaotic experimental time series. One of the major difficulties is that the experimental data contains both the chaotic dynamics of the underlying deterministic system and the random fluctuations produced by stochastic perturbations associated with the experimental process. Using data obtained from a magnetoelastic ribbon experiment we show how a new approach based on topological techniques can be used to obtain a description of the dynamics in terms of subshift dynamics on a finite set of symbols. These topological methods have been developed in a way that allows for the inclusion of experimental error and the existence of bounded noise.

1 Introduction

There has been considerable effort within the scientific community to develop methods to determine whether a given dynamical system is chaotic (see [1] and references therein). On the mathematical side three issues make rigorous analysis of chaotic dynamics difficult. The first is that one is dealing with global nonlinearities making it difficult to obtain the necessary analytic estimates. The second is that the individual solutions are inherently sensitive to the initial conditions. Finally, the objects of interest, namely invariant sets, can undergo dramatic changes in their structure due to local and global bifurcations. The problem is dramatically more complicated in the setting of experimental systems because of the introduction of noise, parameter drift, and experimental error.

In a recent paper [8] we introduced new topological techniques for the analysis of time series which, at least, on the theoretical level can be used to overcome these difficulties. As will be shown in this paper, these techniques can be successfully applied in the context of an actual physical system, a magnetoelastic ribbon subject to a periodically oscillating magnetic field. The actual implementation will be described below. For the moment we remark that our ideas are extensions of the numerical methods developed in [5, 6, 7] along with a reinterpretation of what is an appropriate embedding theorem [9, 3, 2] to justify the use of time delay reconstructions.

At the basis of our approach are three assumptions. The first is that the dynamics of the physical system can be represented by a continuous map

$$f : X \times \Lambda \to X$$

where X represents the phase space and Λ the experimentally relevant range of parameter space. The second is that we are trying to describe the dynamics of an attractor for f in X. The third involves the relationship between the physical phase space and the values observed by the experimentalist. In particular, we allow the experimental observation to be represented as a multivalued map $\theta : X \to [\alpha_x, \beta_x] \subset \mathbf{R}$ where $|\alpha_x - \beta_x|$ may be thought of as an upper bound for the experimental error. However, we also assume that there is a continuous map $\gamma : X \to \mathbf{R}$ such that $\gamma(x) \in \theta(x)$ for all $x \in X$. One may view γ as representing the "true" measurement of the system. We hasten to point out that we are only assuming the existence of such a γ, but never assume that it is known. We should also point out that if it is impossible to choose θ and γ as above, then for some points in the physical phase space arbitrarily small changes in the physical system must lead to arbitrarily large changes in measurements.

To describe the output of our method it is necessary to recall that a *transition matrix* A on k symbols is a $k \times k$ matrix whose entries a_{ij} take values of 0 or 1. Given A one can define a subset of the set of bi-infinite sequences on k symbols,

$$\Sigma_A := \{s = (s_n)_{n=-\infty}^{\infty} \mid s_n \in \{1, 2, \ldots, k\} \text{ and } a_{s_n, s_{n+1}} = 1\}.$$

Let $\sigma : \Sigma_A \to \Sigma_A$ denote the shift dynamics $\sigma(s)_n = s_{n+1}$.

If we choose the dimension of the reconstruction space to be d, then applying our method results in a finite collection of regions N_i, $i = 1, \ldots, k$ in $\mathbf{R}^d$ and an $k \times k$ transition matrix A for which the following conclusion can be justified [8]. Given any sequence $\{\lambda_n\} \subset \Lambda$ and any element $s \in \Sigma_A$ there exists an initial condition $x \in X$ such that

$$\theta(f^n(x, \lambda_n)) \times \theta(f^{n+1}(x, \lambda_{n+1})) \times \cdots \times \theta(f^{n+d}(x, \lambda_{n+d})) \cap N_{s_n} \neq \emptyset.$$

In other words, given any sequence of perturbations in the parameter settings, there exists an intial condition such that, up to experimental error, the reconstructed dynamics describes the observed physical dynamics.

2 Experimental Setup

The magnetoelastic ribbon is a thin strip of material with the property that its Young's modulus varies with the strength of an applied magnetic field. A region of uniform magnetic field was created by the use of three Helmholtz coils. The ribbon was placed in the uniform magnetic field, and clamped from the bottom. The ribbon and Helmholtz coils were encased in a Plexiglass box. The box was placed upon a vibration isolation table, and the entire apparatus was in a temperature-controlled, sealed room. Thus environmental effects were minimized. Nevertheless, the system was extremely sensitive, and thus a significant amount of error needed to be taken into account when doing the calculations. An oscillating magnetic field was applied vertically. When the magnetic field strength is within a certain range, the ribbon will buckle under its own weight. Under these conditions, the ribbon will oscillate back and forth as its stiffness changes. Depending upon the strength of the applied uniform field, and the strength and frequency of the applied oscillating field, as well as the physical characteristics of the ribbon, the motion of the ribbon may exhibit a wide variety of different behaviors. Due to the nonlinear relationship between Young's modulus and the strength of the applied field, the motion of the ribbon may be chaotic. The position of the ribbon once per driving period was investigated.

The data set consisted of 100,000 consecutive data points $\{v_n \mid n = 1, \ldots 100,000\}$ taken from voltage readings on the photonic sensor, sampled at the drive frequence of 1.2 Hz. The voltage readings were measured up to 10^{-3} volts.

3 Implementation of Our Method

In an attempt to provide a concise and coherent description of our method we will present it in the context of our analysis of the above mentioned ribbon data. For an abstract mathematical description of the method the reader is referred to [8]. We selected 30,000 data points $\{v_n \mid n = 30,000, \ldots, 60,000\}$ from our data set. We chose a reconstruction dimension of 2 producing the reconstruction plot of $U := \{u_n = (v_n, v_{n+1})\} \subset \mathbf{R}^2$ indicated in Figure 1.

In order to produce nontrivial topology for our reconstructed system we divided $\mathbf{R}^2$ into a grid of squares with each side of length 0.0106 volts. Let $\mathcal{G}$

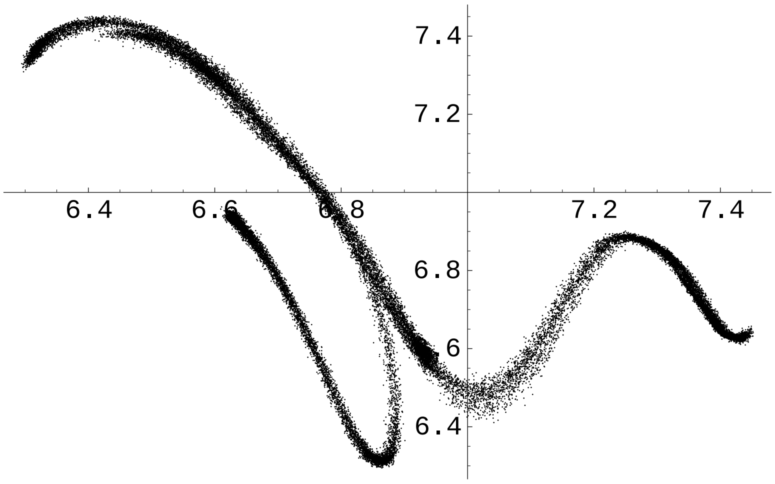

Figure 1: Time delay plot of $u_n = (v_n, v_n + 1)$, $n = 30,000, \ldots, 60,000$, where v_n is the nth voltage.

denote the set of squares which contain a point $u_n \in U$. Let $Y \subset \mathbf{R}^2$ denote the region determined by this collection of squares (see Figure 2).

The next step is to define a dynamical system on Y. This dynamical system is supposed to capture the observable dynamics of the experimental system. Since we know that the physical system is subject to noise and experimental error the derived dynamical system must be very coarse. With this in mind we shall not try to describe the dynamics on any scale smaller than that of the squares in $\mathcal{G}$ and our dynamical system will take the form of a multivalued map $\mathcal{F}$ which takes squares to sets of squares.

To be more precise, let $G \in \mathcal{G}$ and let $\{u_{\alpha_i} \mid i = 1, 2, \ldots, I\} \subset U$ be the set of points which lie in G. From the time series we know that

$$u_{\alpha_i} = (v_{\alpha_i}, v_{\alpha_i+1}) \mapsto (v_{\alpha_i+1}, v_{\alpha_i+2}) = u_{\alpha_i+1}$$

Let $G_i' \in \mathcal{G}$ such that $u_{\alpha_i+1} \in G_i'$. Then up to first approximation we will require that $G_i' \in \mathcal{F}(G)$. Unfortunately, this definition is not sufficient. One reason is that there may be very few samples in the grid square G, so that G_1', G_2', ..., G_I' are isolated squares far apart from each other. We would like $\mathcal{F}(G)$ to be a connected set and to capture all possible images of points of G, not just ones for which we have samples from the time series. Therefore, we include all grid squares contained in the smallest rectangle enclosing G_1', G_2',

Figure 2: Squares with edges of length 0.0106 volts that contain points $u_n \in U$ of the time delay reconstruction.

$\dots$, G'_I in $\mathcal{F}(G)$. However, sometimes this is still not enough. This is because the images of four squares meeting at one point may not intersect which prevents the map $\mathcal{F}$ from having a continuous selector. We deal with this problem in the following way. For each grid point we look at images of four grid squares which meet at that point. If they do not intersect, we increase each image by the set of all squares which intersect the set representing it. We iterate this process until there are no empty intersections. Finally, since we want $\mathcal{F}$ act on $\mathcal{G}$, we intersect each image of a grid square with $\mathcal{G}$.

By means of this procedure we have constructed a multivalued map $\mathcal{F}$ which we believe provides outer limits on the observable dynamics of the experimental system. Trajectories in this dynamical system consist of sequences of squares of the form $\{G_i \in \mathcal{G} \mid G_{i+1} \in \mathcal{F}(G_i)\}$.

We must now face the issue of what dynamics is represented by $\mathcal{F}$. To do this we must make several slight theoretical digressions. Entirely ignoring the question of the magnetoelastic ribbon for the moment, let $g : \mathbf{R}^n \to \mathbf{R}^n$ be an arbitrary continuous map. Recall that $S \subset \mathbf{R}^n$ is an *invariant set* of g if for every $x \in S$ there exists a bi-infinite sequence $\{x_i\}_{i=-\infty}^{\infty} \subset S$ such that $x = x_0$ and $x_{i+1} = g(x_i)$. While invariant sets are the object of interest in dynamical systems, they can be extremely difficult to study directly since they may change their properties dramatically through various local or global bifurcations. For this reason we shall make use of the following notion. A closed bounded set $N \subset \mathbf{R}^n$ is an *isolating neighborhood* if the maximal invariant set in N does not intersect the boundary of N. It is easily shown that if N is an isolating neighborhood for the dynamical system generated by g, then it is an isolating neighborhood for sufficiently small perturbations of g.

Returning to the magnetoelastic ribbon we now look for isolating neighborhoods in Y under the multivalued dynamical system $\mathcal{F}$. We begin by choosing $\mathcal{C}_0 \subset \mathcal{G}$. There are a variety of criteria that can be used in choosing $\mathcal{C}_0$, the important point is that it must be a strict subset of $\mathcal{G}$. We now begin the following procedure. Define

$$\mathcal{C}_1 = \mathcal{C}_0 \cap \mathcal{F}(\mathcal{C}_0) \cap \mathcal{F}^{-1}(\mathcal{C}_0)$$

where $\mathcal{F}^{-1}(\mathcal{C}_0) := \{G \in \mathcal{G} \mid \mathcal{F}(G) \cap \mathcal{C}_0 \neq \emptyset\}$. Now delete a component of $\mathcal{C}_1$ which touches the boundary of $\mathcal{C}_0$ relative to Y. This two step procedure is repeated until $\mathcal{C}_{n+1} = \mathcal{C}_n$. The resulting set $\mathcal{C}_n$ is an isolating neighborhood for $\mathcal{F}$ (see Figure 3). Observe that $\mathcal{C}_n$ consists of 4 disjoint sets labelled N_i, $i = 1, \ldots 4$.

Returning yet again to the theoretical level we need to resolve the following issue. We can compute isolating neighborhoods, but it is the structure of the corresponding isolating invariant set that we are interested in. To pass from isolating neighborhoods to the structure of the invariant set we will use the Conley index [4]. We only need the following small portion of the theory for our purposes. Given an isolating neighborhood N of g, a pair of closed bounded sets (K, L) with $L \subset K \subset N$ is an *index pair* if the following conditions are satisfied:

1. $x \in K$ and $g(x) \in N$, then $g(x) \in K$;
2. $x \in L$ and $g(x) \in N$, then $g(x) \in L$;
3. $x \in K$ and $g(x) \notin N$, then $x \in L$;
4. the maximal invariant set in N is a subset of the interior of $K \setminus L$.

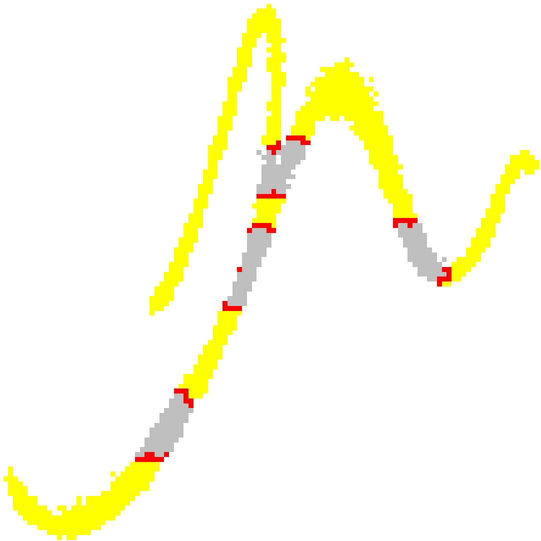

Figure 3: The four shaded regions labelled $N_1, \ldots N_4$ make up the set $\mathcal{C}_n$. The red regions on the boundary of the N_i are L.

The importance of an index pair is that the homology groups $H_*(K, L)$ and a homology map $\tilde{g}_* : H_*(K, L) \to H_*(K, L)$ induced by g are invariants of the maximal invariant set contained in N. Furthermore, if under a change in the dynamics N remains an isolating neighbhorhood then the homology group and map does not change.

Returning to the multivalued dynamics of $\mathcal{F}$, we produce an index pair as follows. Let L consist of the elements of $\mathcal{F}(\mathcal{C}_n)$ which touch the boundary of $\mathcal{C}_n$ relative to Y. Let $K = \mathcal{C}_n \cup L$. Then, (K, L) is an index pair for $\mathcal{F}$. Figure 3 indicates the resulting index pair.

We now compute $H_*(K, L)$ using $\mathbf{Z}_2$ coefficients and determine that it is a four dimensional vector space and the corresponding map on homology is the matrix

$$A = \begin{bmatrix} 0 & 0 & 0 & 1 \\ 0 & 1 & 1 & 0 \\ 1 & 0 & 0 & 0 \\ 0 & 1 & 1 & 0 \end{bmatrix}.$$

At this point we can describe the essential difference between this development and that based on the embedding theorems mentioned earlier. The embedding theorems assume that the points $U \subset \mathbf{R}^2$ actually represent elements of trajectories of a fixed smooth map on a subset of $\mathbf{R}^2$ and that the dynamics of this map can now be embedded into the dynamics of the physical system. We make no such assumption. Instead we use the existence of the continuous map $\gamma : X \to \mathbf{R}$ to lift the algebraic topological quantities associated with A to X. This allows one to conclude [8] that A represents a transition matrix for a symbolic coding of the dynamics in the physical phase space.

At the risk of being redundant this implies that given any small random environmental effects on the experiment and any sequence $b \in \Sigma_A$, there exists an initial condition for the physical system such that using our observational method the trajectory will, up to experimental error, pass through the regions labelled N_i, $i = 1, \ldots, 4$ in the manner indicated by b. For example the sequence $\ldots 4132224134132413 \ldots$ lies in Σ_A and hence there exists an intial condition for the ribbon such that our observations would indicate that up to experimental error its reconstructed trajectory lies in the following sequence of regions

$$N_4 \to N_1 \to N_3 \to N_2 \to N_2 \to N_2 \to N_4 \to N_1 \to N_3 \to N_4 \to N_1 \to \cdots$$

4 Conclusions

Our method provides an explicit description in terms of symbolic dynamics of the chaotic behavior of the magnetoelastic ribbon. This is a much finer description of the dynamics that is usually presented from experimental data. For example, given A it is easy to conclude that the topological entropy for the ribbon must be greater than $\ln 1.4656$.

Two other methods that are commonly used to analyze chaotic data involve the approximation of Lyapunov exponents or the determination of a fractal dimension. Both the determination of the Conley index and of Lyapunov spectra require some similar assumptions:

1. the data provided is a reasonable approximation to what one would obtain if measurements could be performed for an infinite amount of time;

2. the phase space reconstruction has given a good approximation to the underlying dynamics;

3. the underlying system is assumed to be governed by a deterministic set of equations.

For the computation of Lyapunov spectra one must assume that the reconstruction has been done in a sufficiently high dimensional space. In our setting this is no longer an assumption. In particular, whenever one computes nontrivial algebraic topological quantities the resulting conclusions about the dynamics are correct. Of course, if one chooses a dimension that is too low, then the resulting multivalued map will either not contain any nontrivial isolating neighborhoods or the corresponding algebra will be trivial. It is easy to construct examples where the embedding fails but the algebra is still nontrivial.

An even more fundamental difference is that the Lyapunov exponent is a global quantity that is highly dependent on noise and very sensitive to perturbations. What's more a lot of questions about Lyapunov exponents are unanswered. How much noise and parameter drift can there be before any estimate of the exponents becomes meaningless? The Lyapunov exponent is limited in what it can tell us about the dynamics. In its traditional form, it is a global quantity that tells nothing about what sort of changes occur in the local dynamics. Also it does not provide us with significant information for use in a symbolic dynamics. This sort of description which we provide may be useful in applications such as control theory.

On a more concrete level we performed Lyapunov exponent calculations and embedding dimension calculations on this data set. The dominant Lyapunov exponent seemed to be roughly 0.48. However, under reasonable parameter regimes, the computed Lyapunov exponent ranged between 0.45 and 0.99. This indicates that computation of the Lyapunov exponent is extremely parameter dependent.

The same problems exist with a determination of fractal dimension. The dimension tells us little about the underlying dynamics. In addition, a reasonable estimate of dimension is very difficult to compute from experimental data. In theory, because it is a limit that is reached only with infinite data, the fractal dimension is not a computable object.

Measurement of the embedding dimension also yielded somewhat questionable results. This algorithm identifies the percentage of false nearest neighbors for a given embedding dimension. Although we found that an embedding dimension of three should be sufficient, the minimum embedding dimension differed greatly depending on our criteria for identification of a false nearest neighbor. In some analyses, it seemed an embedding dimension of 5 was necessary to decrease the percentage of false nearest neighbors to less than 5%. As noted before, the symbolic dynamics approach implemented here does not have these problems.

Finally, our approach appears to provide robust repeatable conclusions. As was mentioned earlier we collected 100,000 data point during the experiment. We repeated the above mentioned proceedure using the points $\{v_n \mid n = 70,000, \ldots 100,000\}$. As one can see from Figure 4 there are observable differences in this collection of data points. After applying our procedure we obtain the index pairs indicated in Figure 5 which are also slightly different. However, on the level of the algebra and hence the symbolic dynamics we obtained the same transition matrix

$$A = \begin{bmatrix} 0 & 0 & 0 & 1 \\ 0 & 1 & 1 & 0 \\ 1 & 0 & 0 & 0 \\ 0 & 1 & 1 & 0 \end{bmatrix}.$$

In conclusion, we have proposed a theoretically justified and experimentally validated method which takes time series data as an input and produces the output of a transition matrix and its associated regions in reconstruction space which may be used to rigorously verify chaos, analyze and identify invariant sets, and determine properties of the global dynamics above the noise level. The power in this method is that the noise has been taken into account before any analysis is done. All analysis is on a scale where the results of the analysis are robust with respect to noise. Where commonly used, quantitative measures of chaos (such as Lyapunov exponent estimates) may fail because of sensitivity in the analysis. In contrast verification of chaos from analysis of the transition matrix is robust.

Acknowledgements: The first author's research was partially supported by NSF grant DMS-9505116.

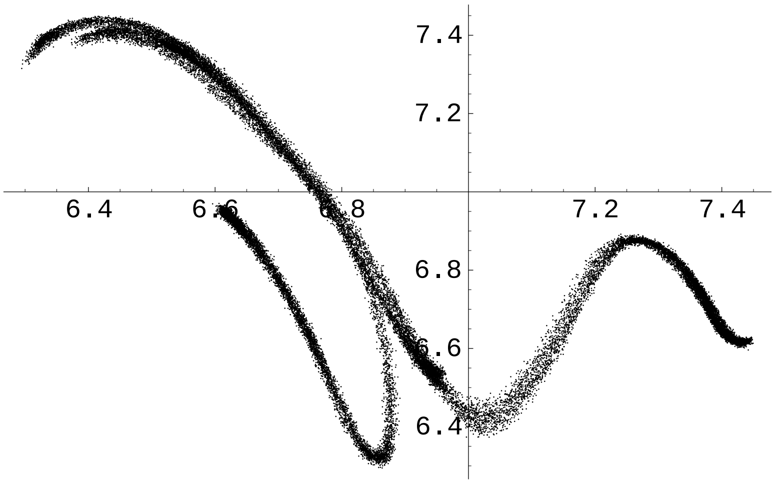

Figure 4: Time delay plot of $u_n = (v_n, v_n + 1)$, $n = 70,000, \ldots, 100,000$, where v_n is the nth voltage.

References

[1] H. Abarbanel, *Analysis of Observed Chaotic Data*, Springer, New York, 1996.

[2] M. Casdagli, T. Sauer, J. A. Yorke, Embedology, *J. Stat. Physs*, **65** (1991) 579-616.

[3] J.-P. Eckmann and D. Ruell, Ergodic theory of chaos and strange attractors, *Reviews of Modern Physics*, **57** (1985) 617.

[4] L. Arnold, C. Jones, K. Mischaikow, G. Raugel, *Dynamical Systems Montecatini Terme 1994*, R. Johnson, ed., Lect. Notes Math. 1609, Springer, 1995.

[5] K. Mischaikow and M. Mrozek, Chaos in Lorenz equations: a computer assisted proof, *Bull. AMS*, 33 (1995) 66-72.

[6] K. Mischaikow and M. Mrozek, Chaos in Lorenz equations: a computer assisted proof. Part II: Details, *Mathematics of Computation*, to appear.

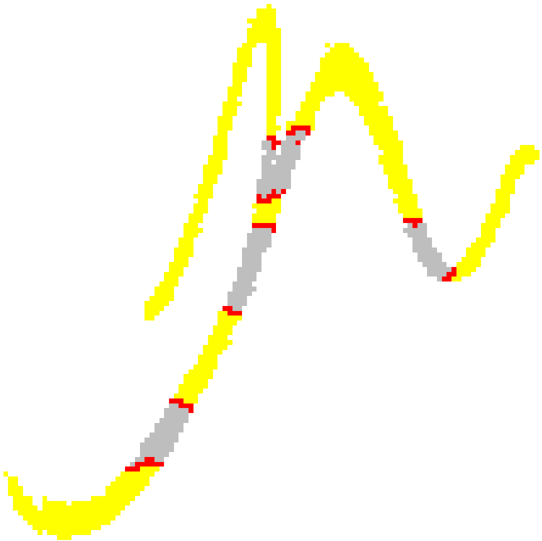

Figure 5: The four shaded regions labelled $N_1, \dots N_4$ make up the set $\mathcal{C}_n$. The red regions on the boundary of the N_i are L.

[7] K. Mischaikow, M. Mrozek, and A. Szymczak, Chaos in Lorenz equations: a computer assisted proof, Part III Classical Values, in preparation.

[8] K. Mischaikow, M. Mrozek, A. Szymczak, and J. Reiss, *From Time Series to Symbolic Dynamics: An Algebraic Topological Approach*, preprint http://www.math.gatech.edu/ mischaik/papers/paperlist.html

[9] F. Takens, Detecting strange attractors in turbulence, *Dynamical Systems and Turbulence, Warwick 1980*, eds. D. Rand and L. S. Young, eds. p. 366 Springer, Berlin, 1981.